International Journal of Pressure Vessels and Piping 205 (2023) 104964

Contents lists available at ScienceDirect

International Journal of Pressure Vessels and Piping

journal homepage: www.elsevier.com/locate/ijpvp

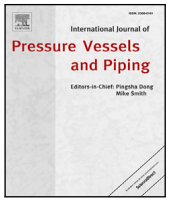

Model-experiment comparison for transverse loading of metal–composite ring specimen (Part 1)

Erick Montes de Oca Valle [a,*], Mark Spearing [a], Ian Sinclair [a], Trevor Allen [a], Warren Hepples [b]

[a] University of Southampton, University Road, Southampton, SO17 1BJ, UK
[b] Luxfer Gas Cylinders, Colwick Industrial State, Nottingham NG4 2BH, UK

ARTICLE INFO

Keywords:
Finite element modelling
Pressure vessel
Cohesive elements
Damage tolerance

ABSTRACT

As a building block towards improved understanding and design of Composite Overwrapped Pressure Vessels (COPV), this paper presents simulations and experimental validation of a 3D finite element model for a metal–composite ring structure subjected to quasi-static indentation, used as a proxy for low velocity impact (LVI). The focus of the work is to model composite ply delamination as well as metal–composite separation, using cohesive elements. A methodology is presented to determine the parameters used for the traction-separation law that controls the cohesive elements. The model was calibrated and validated using a hybrid metal–composite ring at reasonable engineering length-scales, corresponding to structures with 159 mm outer diameter and 50 mm length. Each ring specimen was loaded in displacement controlled compression up to 20 mm, *i.e.* the point at which composite delamination and plastic deformation of the metallic layer has occurred. Validation is performed by comparing experimental force–displacement curves, strain fields and damage mechanisms to results obtained from the finite element (FE) model. Results from the numerical modelling are in good agreement with experimental values.

1. Introduction

Composite Overwrapped Pressure Vessels (COPV) are hybrid structures that commonly contain gases in a range of 25–70 MPa and are widely used for different applications, such as medical, self-contained breathing apparatus (SCBA) and transport [1]. Current COPV design standards focus on a range of potential damage and general degradation mechanisms, including unexpected out-of-plane loadings, such as low velocity impact (LVI), which may occur from accidental dropping or cylinder misuse. This type of loading can cause phenomena akin to Barely Visible Impact Damage (BVID) on the composite inner layers and the metallic liner, which complicates the assessment of the load-carrying capacity of the structure after the impact. As such, damage tolerance of these cylinders is of great interest, specially to understand the effect that subsequent damage may have on the structure's fatigue and burst pressure performance.

Low-velocity impacts on COPV have been reported by several authors [1–3]. Kobayashi & Kawahara [4] studied the effect of the composite wrap thickness on the residual structural response of an empty metal lined pressure vessel subjected to quasi-static indentation and LVI. Results suggested that increasing the lower case for Carbon Fibre Reinforced Polymer (CFRP) thickness contributes to an increased initial stiffness and a reduced aluminium liner deformation. Wakayama et al. [3] performed impact tests on filament-wound polymer vessels using three different types of low-modulus pitch-based carbon fibres. Using Computer Tomography (CT) to scan the specimens and observe the depth of the damage caused by different impactor shapes, data suggested that the depth of the damage caused by the impact was indeed correlated with a decrease in residual burst pressure strength. Blanc-Vannetet al. [5] studied the effect of increasing impact energies on empty, thick polymer liner pressure vessels, and reported a reduction in residual burst pressure due to higher impact energies. Subsequent reductions in fatigue life of metal-lined pressure vessels have also been reported as a result of low-velocity impacts [6,7]. Results indicate that a deeper composite damage, as a consequence of increasing impact energies, contributes to a greater reduction in the fatigue life of the cylinder.

Composite rings have been also used as an alternative experimental approach to investigate composite pressure vessels or tubes. Ha & Jeong [8] used rings to investigate the influence of winding angles on the through-thickness properties of thick wound filament composite tubes. Residual strain measurements were reported under various winding angle configurations. Eggers et al. [9] reported the structural force–displacement response and damage mechanisms of filament-wound

* Corresponding author.
E-mail address: emdo1g15@soton.ac.uk (E. Montes de Oca Valle).

https://doi.org/10.1016/j.ijpvp.2023.104964
Received 20 June 2022; Received in revised form 13 April 2023; Accepted 20 April 2023
Available online 25 April 2023

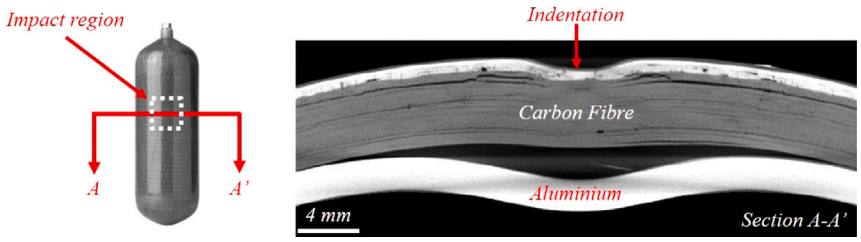

Fig. 1. CT image of metal–composite delamination within a COPV after quasi-static loading [20].

composite rings under hoop tensile and radial compression loads. Specimens were manufactured with different winding angles, diameter-to-thicknesses and stacking sequences. Similarly, Weerts et al. [10] investigated residual strains in thick-walled composite cylinders with a polymer liner subjected to compression loads. These approaches used quasi-static tests to induce damage in the specimens, which has been reported to be a valid approximation to LVI [4,11–13].

Complementary to experimental investigation of pressure vessels, numerical modelling is an attractive option to reduce costs, testing time and it allows the possibility to study damage development during load application. Changliang et al. [14] developed a finite element (FE) damage model of the composite layers of a hybrid pressure vessel. Results for fibre and matrix fracture on the outer layers of the pressure vessel were reported from this model with good agreement to experimental results. Kim et al. [7] investigated the effect that induced flaws in the outer composite layers have on the fatigue performance of metal-liner COPV. Results suggested that a deeper flaw contributes to a greater reduction in a cylinder's fatigue life. No delamination or fibre/matrix damage were considered in Kim's model, however good agreement between experimental and modelling results was reported. A different approach was taken by Han et al. [15] who modelled a hybrid metal–composite vessel under free fall impact. This FE 3D model used Hashin's criterion to determine fibre fracture, matrix crack and delamination in the inner layers of the cylinders and, thus, it was possible to suggest whether the cylinder could be re-used or not. This model was later used to predict damage in COPV in a car-to-car collision simulation [16]. Kobayashi et al. [17] used FE modelling to evaluate residual burst pressure of hybrid metal–composite pipes. Results show residual stresses after burst pressure loading and residual burst strength after low-velocity impact. Both models showed good agreement with experimental results for composite damage after impact, however it is not clear as to what extent of damage would render the cylinder unusable. These models were developed using a microscale approach, however further COPV modelling has been reported using ply-to-ply approaches for more mesoscale modelling focusing on delamination between CFRP layers and liner separation resulting from impact and internal pressure loads [18,19].

The modelling approaches referenced above were focused on investigating damage in the composite layers of the vessels and only few studies have assessed damage in the liner [10,18], and these are on polymer liner pressure vessels. It has been suggested that as a result of LVI, hybrid metal–composite pressure vessels exhibit a separation of the metal–composite interface and a residual indentation in the aluminium liner [1], similar to that shown in Fig. 1. Allen et al. [20] performed quasi-static point indentation tests on hybrid COPV as an approach to replicating LVI. Force–displacement curves were obtained to analyse the structural response of the whole cylinder under this loading (Fig. 2a) and study it in relation to the residual depth observed in the metal liner. Results suggested that there is a correlation between the depth of the dent and the post impact fatigue life of the specimen (Fig. 2b). Based on the results, the effect of reducing the amount of residual plastic deformation on the liner should be investigated.

This is the first of a set of two papers presenting the methodology to investigate the damage on the metal liner of Type 3 pressure vessels. In the present paper, Part 1, a numerical model of a hybrid metal–composite ring is developed and presented. The methodology and estimated properties described in this paper are later used to develop a 3D full-cylinder FE model which is presented in Part 2. The aim of this model is to estimate CFRP and metal–composite interface properties to predict delamination and the residual indentation in the metal layer. Previous modelling investigations on hybrid pressure vessels use an ideal metal–composite bond or take reference properties from experimental tests that have been performed on plates [10,15]. However, given the geometry and the residual stresses contained in a COPV, such properties have been not assumed in this work. The current FE model contains cohesive elements that are used to estimate the interface fracture toughness and strength of the metal–composite bond. Estimated properties will be then referenced to develop a full COPV FE model that can be used for design optimisation considering minimisation of the residual dent as one of the design objectives.

Table 1
Material properties of the 6061-T6 Aluminium.

Young's modulus (E)	Ultimate tensile stress (σ_{uts})	Yield stress (σ_y)	Poisson's (ν)
69 GPa	310 MPa	276 MPa	0.3

Table 2
Material properties for the composite plies.

E_{11}	$E_{22} = E_{33}$	G_{12}	ν_{12}
139 GPa	6.63 GPa	3.78 GPa	0.28

2. Methodology

2.1. Ring specimen FE model

A ply-level modelling approach was selected to model the composite wrap, having a total of six plies with hoop and helical layers modelled individually. Details regarding fibre orientations in the model are discussed in further sections. Material properties of the composite wrap used in the model can be found in Table 2. For this model, delamination within the CFRP and the metal–composite interfaces are the only damage mechanisms investigated, that is, no fibre or matrix fracture is considered.

The FE model was developed in the commercial software Abaqus CAE®. Based on the known structure of the physical specimen, the ring is divided into different layers, one corresponds to the metal ring of the structure and others correspond to the CFRP layers (Fig. 3). Each layer consist of solid (C3D8R) elements with one element through the thickness, except for the metal ring which has three elements through its thickness. The indenter and the support used to enforce the delamination were modelled using rigid (R3D4) elements. The aluminium was modelled as an elastic-perfectly plastic material, with the properties given in Table 1. The composite was modelled as being elastic, other than allowing for the possibility of delamination, as described below.

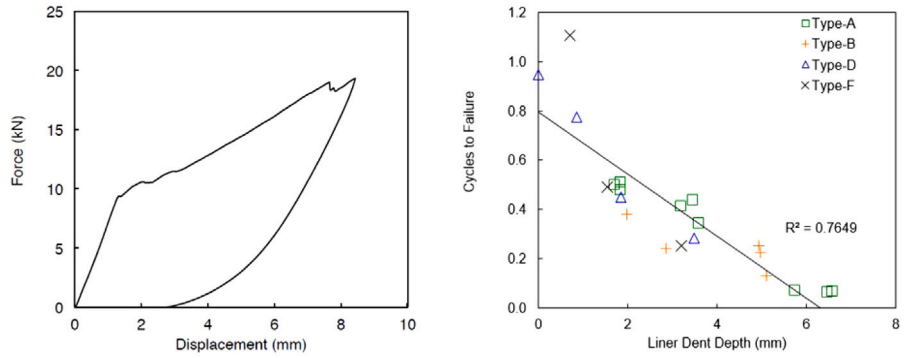

Fig. 2. COPV quasi-static loading behaviour: (a) Force–displacement curve response after indentation loading; (b) Correlation between liner dent depth and fatigue life [20].

To model the metal–composite interface as well as delamination occurring within the CFRP layers, cohesive elements were used. These finite elements are typically used in delamination problems and they are defined by a traction separation law [21]. In between each section of the ring model, 0.01 mm thick cohesive elements (COH3D8) are used, except for the section between the helical layers which are joined together using a tied contact for simplicity, as the delamination observed on these regions is limited in comparison to that shown in between the hoop layers. Different cohesive element interfaces are embedded in this model, of which one contains unique properties for the metal–composite interface. The rest of the interfaces contain the same properties to predict the delamination within the CFRP layers. Contact was defined in-between layers to ensure no material penetration occur in the case of cohesive element deletion (delamination). Geometric and meshing details of the FE ring model are shown in Fig. 3.

Cohesive element properties were defined through parametric investigation of the parameters that define the traction-separation, *i.e.* interface strength (τ^0) and interface toughness (G_c) in modes I and II. These parameters define the traction separation law which determines the cohesive layer behaviour and ultimate interface delamination. Considering that the metal–composite interface is of high interest due to its possible effect on the residual dent development, three values where proposed for each cohesive element parameter *i.e.* three traction-separation laws for each mode. For the composite interface properties, only one traction-separation law was proposed. Despite the interface properties in the metal–composite interface of the cylinder have not been mentioned in literature, we have assumed that they are comparable to those mentioned in similar studies [22,23]. As such, the purpose of this study to identify the values that produces a result that reasonably approximates the overall structure's behaviour compared to the experimental data.

To overcome convergence difficulties it was decided to use the Abaqus/Explicit solver [24]. The solution is divided into two different steps: loading and unloading. The former refers to the compression of the ring specimen, and the latter refers to load release. Load is applied through 20 mm controlled displacement of the upper rigid support. The loading point velocity is 0.04 m/s and a mass scaling factor of $1e3$ is used [24]. There are two mesh refinement levels on the structure, upper and lower (Fig. 3). The upper half of the ring has a mesh size of 10 mm and it was modelled to add an elastic stiffness response, thus, no cohesive elements were included in this region of the model and the plies are joined using a tied contact. The lower half of the ring has a mesh size of 0.6 mm, which ensures at least five elements are used to model the cohesive region [25].

2.2. Ring specimen indentation test

An analogous experimental test to the FE model was performed. Ring specimens were manufactured by cutting a 9-litre COPV into 50 mm length slices. Total ring diameter was 159 mm, with a 2.2 mm liner thickness and 4.6 mm CFRP thickness. The specimens were loaded in compression using an electro-mechanical testing machine, a v-shaped loading support and a longitudinal bar (r = 8 mm) that induced indentation across the specimen length, in this way the delamination should remain approximately constant through the length of the specimen, *i.e.* creating an essentially 2D problem (Fig. 4). The loading procedure is similar to the quasi-static indentation test presented in [20] and analogous to the FE model, *i.e.*, load is applied using a loading and an unloading step.

Digital Image Correlation (DIC) was used to measure strains that can be compared to the FE model. Furthermore, this tool was also used to indicate the onset of damage that may not be apparent by direct imaging. Two LaVision E-lite cameras in stereo configuration were used to record images [26], and each camera was equipped with a 105 mm lens. The region on which the cameras are focused, *i.e.* field of view FoV, was defined based on the area where the maximum delamination and metal residual indentation are expected (Fig. 4). The speckle pattern was defined with a white matte paint as a background. Then, black was applied using a spray at a 1 m distance from the specimen. As suggested in the literature [26], each speckle covered 3–5 pixels. The final speckle pattern is showed in Fig. 4.

3. Results

3.1. Experimental results

Data collected from the experiment includes force–displacement (F–d) curves, delamination images and strain fields. Results for load are presented in normalised format due to proprietary sensitivities. The same normalisation value is used for the experiments and FE model. Fig. 5 shows the F–d curves response of the ring specimen which exhibits several load drops during loading (points A, B, C). Similarly, Fig. 5 shows the nominal strain (ϵ^*_{xy}) fields obtained from DIC used to track delamination (Fig. 5a, 5b and 5c). A yellow dotted line was added as a reference to differentiate between the aluminium and the CFRP materials. When comparing the strain values to the F–d curve, it was confirmed that the load drops correspond to significant delamination events within the ring. Points A and B, for instance, relate to delamination within the CFRP layers, whilst point C corresponds to metal–composite delamination. The curve indicates that after metal–composite delamination there is a marked loss in overall stiffness, *c.f.* the onset of composite delamination. Point D is the maximum displacement application at the end of the compression step, at which ϵ_{xx} strains were measured on the aluminium ring using DIC (Fig. 5d). This data can be directly compared to that obtained from the FE model. Point E shows the end of the load release step and the residual indentation on the aluminium ring. At this point it was difficult to obtain an acceptable strain measurement due to the level of damage induced in the ring, particularly in the composite layer (Fig. 5e).

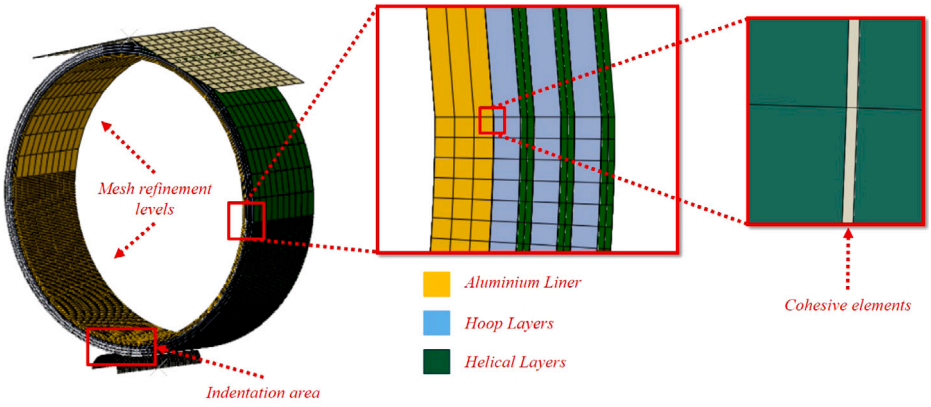

Fig. 3. FE ring model description.

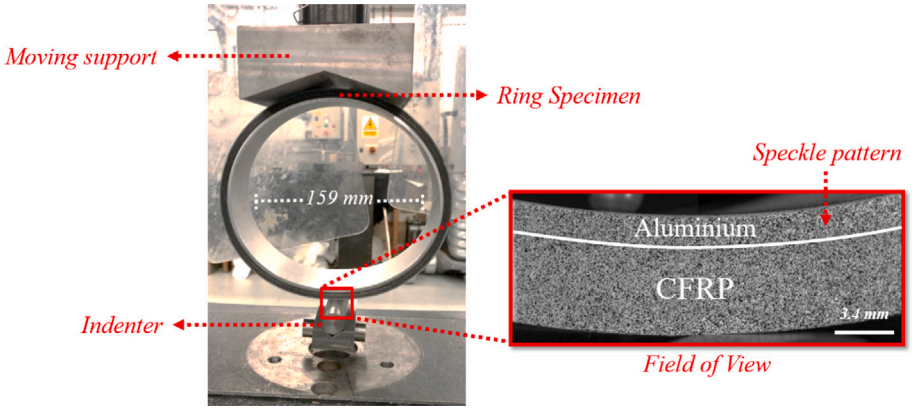

Fig. 4. Ring specimen test setup.

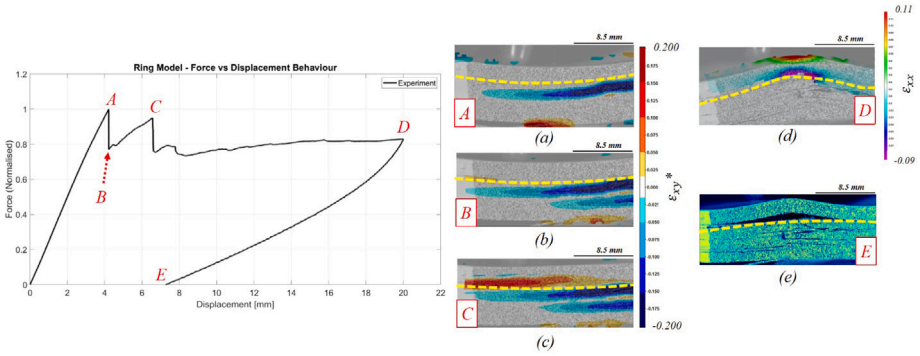

Fig. 5. Normalised experimental force–displacement curve; (a) First major CFRP delamination; (b) Second major CFRP delamination; (c) Metal–composite interface delamination; (d) Maximum compressive load application; (e) Residual indentation (load removal).

3.2. Model calibration & validation

3.2.1. Force–displacement behaviour

F-d curves similar to those obtained from the experimental tests were obtained from the FE model for comparison. The virtual curves exhibit oscillations as a result of the dynamic solution used for the analysis. Fig. 6 shows a comparison between the experimental curve and a result from the FE model. Four main characteristics are observed in the virtual result: an initial elastic response, a first and a second noticeable load drops (points X and Y) and an unloading response (point Z). The initial response exhibits good correlation with the experimental curve. From the model delamination results (Fig. 6a), it was noticed that the first load drop (point X) is related to delamination occurring within the CFRP plies. After this damage, the reaction force remains stable until a second load drop occurs (point Y) which is a consequence of metal–composite delamination and yield of the metal layer (Fig. 6b). Similar to the experimental curve, the FE model behaviour shows that after metal–composite delamination the ring's stiffness can no longer be recovered, although this damage mode occurs almost at the end of the compression step in the simulation. Finally, after load release, the FE curve exhibits a similar final response to that shown in the experiment (point Z) related to the development of the residual indentation (Fig. 6c).

As noted previously, three different simulations were performed using combinations of parameter values shown in Table 3. In this work only the influence of the metal–composite interface fracture toughness variation is presented as it is a combination of interface strength and interface separation [21]. Fig. 7 shows the F-d response of the ring

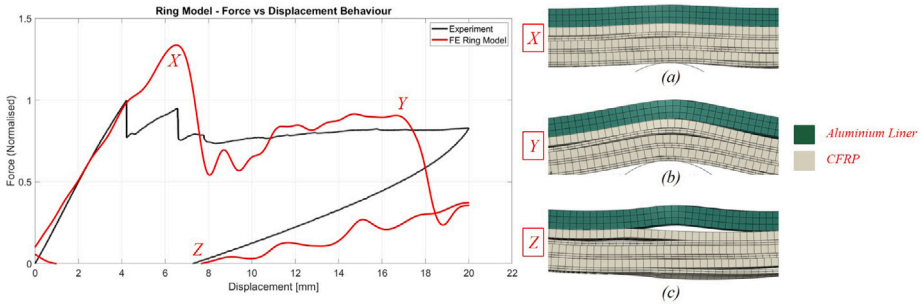

Fig. 6. Normalised force–displacement curve comparison vs. Experiment; (a) Composite delamination; (b) Metal–composite delamination; (c) Residual indentation.

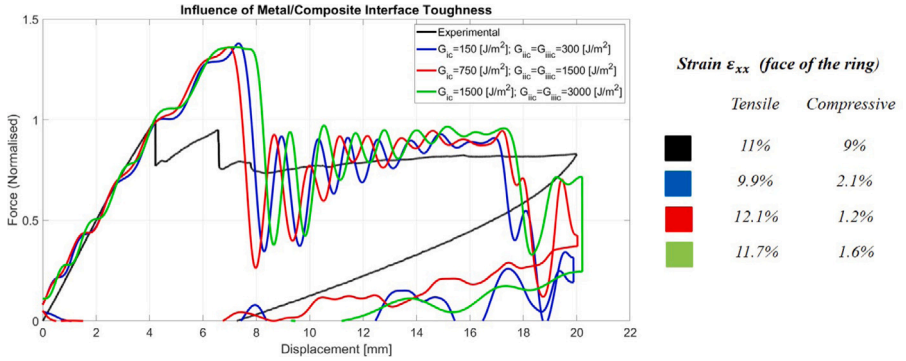

Fig. 7. Ring specimen structural compression response under various metal–composite interface toughness values.

Table 3
Metal–composite interface properties for cohesive elements.

τ_{11}^0 (MPa)	$\tau_{22}^0 = \tau_{33}^0$ (MPa)	G_{Ic} (J/m^2)	$G_{IIc} = G_{IIIc}$ (J/m^2)
10, 20, 30	20, 40, 60,	150, 750, 1500	300, 1500, 3000

specimen under various interface fracture toughness values as well as ϵ_{xx} measurements performed on single nodes corresponding to the inner and outer face of the aluminium layer of the metal ring. It can be observed that, within a range of 750 J/m^2–1500 J/m^2 for G_{ic} and 1500 J/m^2–3000 J/m^2 for G_{iic}, the model is relatively insensitive in terms of the resulting structural response. However, when comparing the ϵ_{xx} results, we find greatest consistency with experimental data using $G_{ic} = 1500$ J/m^2 and $G_{iic} = G_{iic} = 3000$ J/m^2.

3.2.2. Strain measurement results

As indicated in [20] the residual dent formed on a COPV has a strong correlation to the fatigue life of the component and, thus, it can be an indicator of the structure's post impact performance. Therefore, strain measurements were particularly carried out on the aluminium layer to investigate the residual dent development after loading. Fig. 8 shows a comparison of the strain fields on the aluminium liner at the maximum point of compression (end of load step). Two different nodal measurements were compared at the maximum point of deflection on the lateral face of the ring. It can be observed that the tensile strain correlates well to the DIC measurement. However the compressive strain measurement indicates a large difference between the two results. It is likely that the level of delamination occurring adjacent to the metal is affecting the DIC measurements, hence conflating actual continuum strains with crack surface displacements, resulting in a high measured value of the "effective" strain. Fig. 9 shows the experimental and virtual residual indentation observed on the metal layer, which correlates well, in terms of both shape of the metal indent and the damage occurring in the composite.

Following strain investigation on the metal ring, more detailed quantitative point, line and area measurements were made on the face of the FE and the experimental ring specimens for comparison. Additionally, these measurements were made at different applied displacements, *i.e.* measurements were performed at 2, 5, 7, 10, 15, and 20 mm during the loading phase (see Fig. 10).

In order to investigate details regarding the dent formation, similar strain measurements were obtained at different load application levels during the experiment and the simulation. The points at which the measurements were performed are shown in Fig. 10. The first comparison was performed on specific nodal locations.

To perform point measurements using DIC, a specific coordinate was selected in the tensile strain region located two sub-regions lengths from the edge to avoid edge effects (Fig. 11a). The analogous node was selected in the FE model to compare strain measurements through the load application(Fig. 11b). Strain values are normalised by the highest strain value registered on each type of measurement. The point/node comparison though different loads during the experiment/simulation is shown in Fig. 12. It can be observed that there is a good agreement between the two curves, although the FE curve is predicting a slightly higher strain value towards the end. Additionally, strain measurements were performed over a line of points that is placed along the thickness of the metal ring (Fig. 13). In this particular case, the liner thickness was normalised to unity due to proprietary sensitivities. Similar to the point measurements, DIC results were compared to an analogous line of nodes in the FE model through the same applied displacement points. Fig. 14 shows the FE vs DIC measurement comparison at different displacement application levels of the support on the ring. It can be observed that as the support displacement increases (*i.e.* increased ring compression) the agreement between the two measurements improves, especially at the end of the loading step (maximum ring compression). The measurement at 15 mm displacement shows the least agreement between DIC and FE attributable to large oscillations during the simulation as a result of metal–composite delamination.

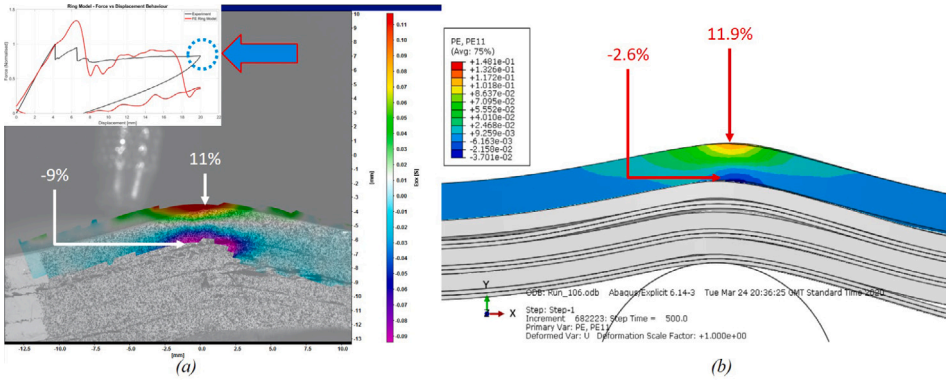

Fig. 8. ϵ_{xx} strain measurements on aluminium ring; (a) DIC; (b) FE ring model.

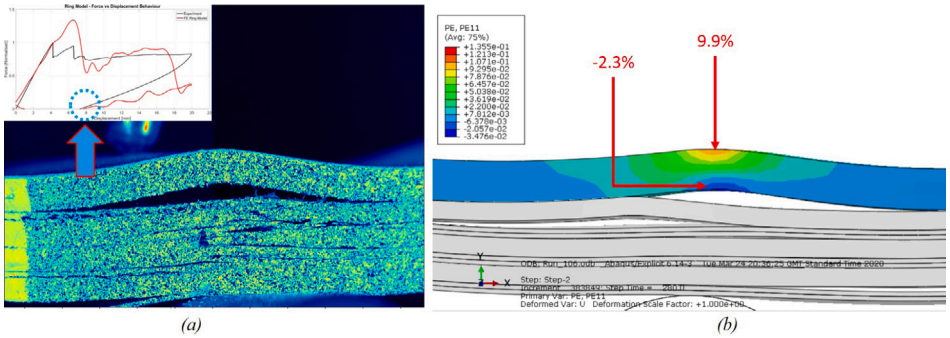

Fig. 9. Residual metal indentation of ring specimen; (a) DIC; (b) FE ring model.

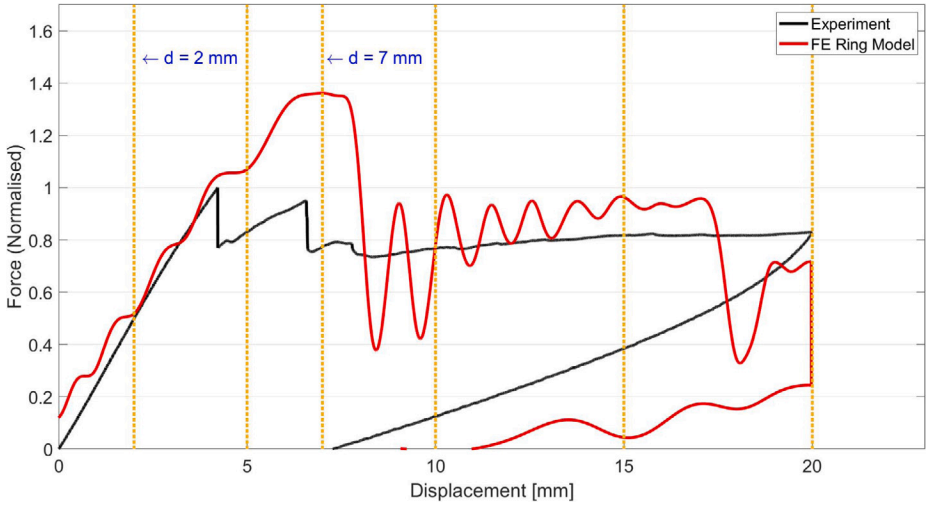

Fig. 10. Reference points for point, line and area strain measurements comparison: DIC vs FE ring model.

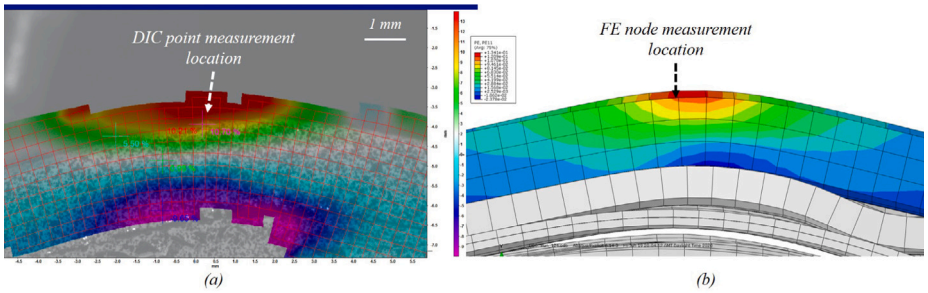

Fig. 11. FE vs DIC ring measurement points.

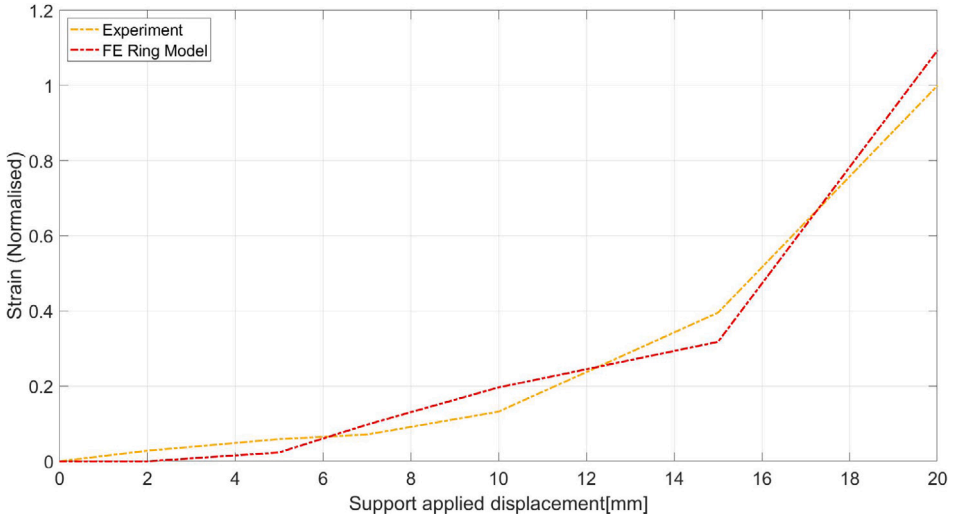

Fig. 12. Point/node measurement comparison plot.

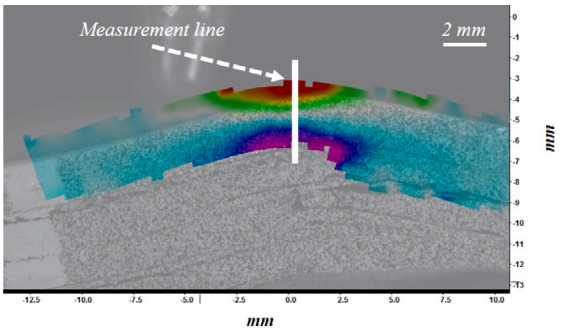

Fig. 13. Line measurement on metal ring.

Finally, area strain measurements were performed. To achieve this, strain values were taken from two different sized areas of the DIC FoV (Fig. 15). Area *A* is 5.22 mm × 1.53 mm and area *B* is 15.2 mm × 1.53 mm. The tensile strain values were averaged and registered for every load increment during the loading step. A similar procedure was performed using the FE model. Fig. 16 shows the resulting plots after comparing the FE and DIC averaged strains during the loading step. It can be observed a good level of agreement is achieved between both sets of results.

4. Discussion

Damage propagation during compression of a hybrid composite ring has been investigated and modelled. Previous approaches of damage investigation of COPV have focused on the use of CT scans and contributed to the assessment of post impact damage. The information collected and presented in Fig. 5 shows the sequence in which damage occurs. The damage sequence starts with major two delaminations within the CFRP layers which produces a load drop in both cases. However after each load drop the structure still shows some stiffness recovery. The third main damage event is the metal–composite interface delamination after which the overall stiffness remains relatively low (Fig. 6c). Additionally, it was observed that the highest metal deformation occurs after the metal–composite delamination. The described damage sequence occurs mainly during the increase in applied displacement, although some additional delamination was observed during the unloading phase. This suggests that the delamination mechanism is mainly driven by mode II delamination rather than mode I, which was previously suggested in [20].

The sequence obtained from the experimental test was used to validate the FE results. Despite simplifications made (*e.g.* no fibre or intralaminar failure) and type of solution (explicit solver) the overall predictions exhibit an acceptable behaviour. When both experimental and virtual F-d curves are compared there is a good degree of overall similarity, with some differences, that might be addressed by subsequent, more refined models. The first load drop from the virtual

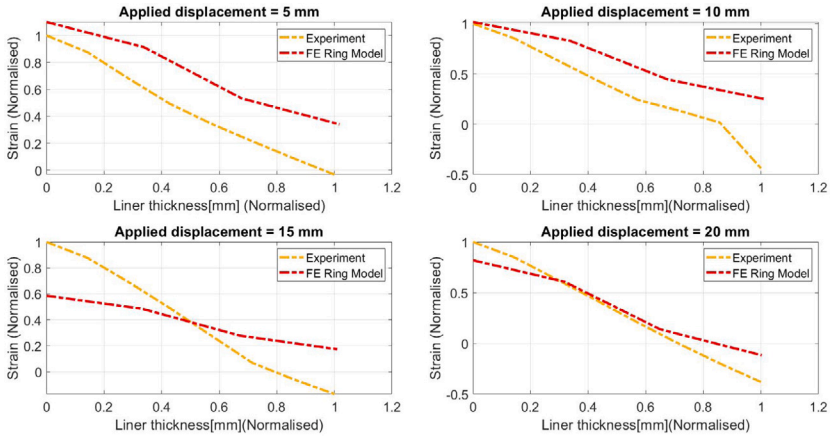

Fig. 14. Line measurements performed at different load application on the ring specimen.

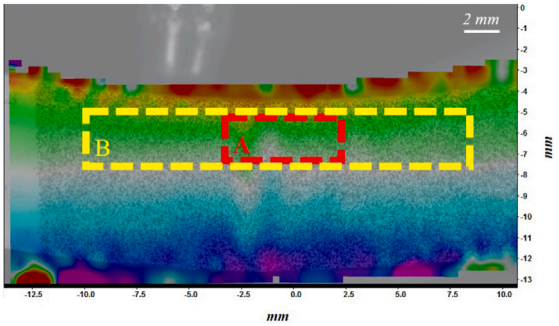

Fig. 15. Areas for strain average measurement on metal ring.

F-d curve corresponds to damage occurring in the composite material, although it occurs during at a point of rapid progression. Following this mechanism, the major damage observed in the FE curve is due to the metal–composite delamination and associated yielding of the metal layer. Finally, the point at which the curves return to zero is similar to that in the experimental curve. The damage propagation sequence shown by the FE model is similar to that observed in the experimental test, however, differences are noticeable due to the high level of oscillations in the model and the *rapid* delamination simulated. Despite the differences and, given the level of damage in the ring specimen, the model exhibits a good representation of the structural response behaviour (shown in the F-d comparison), local strain response and the residual indentation (Fig. 9).

The FE ring model is also used to estimate the properties of the metal–composite interface of the structure. The model was *calibrated* using a range of interface fracture values. The results shown in Fig. 7 suggest that, regarding the overall structural behaviour described by the F-d curves, the model is relatively insensitive to the precise toughness value within a reasonable broad range. Given that the metal dent characteristics are known to be a strong indicator of remaining fatigue life, and hence damage tolerance, particular care should be taken if this is key parameter of interest.

5. Summary and conclusions

In this study a FE model of a hybrid metal–composite ring structure was presented and validated through experimental work. Metal-composite interface properties were estimated by comparing force–displacement structural behaviour and strain measurements obtained from experiments and FE modelling. The FE ring model predicts structural behaviour with a good level of agreement to the experimental observations. Residual indentation prediction was correlated through mechanical visualisation, chronological comparison and strain measurements.

Strain measurements sufficiently removed from delaminations exhibited strong agreement between the experimental and FE results. Validation activities are presented in relation to strain measurements on the ring specimen using DIC, which are compared to those obtained from the FE model. Only tensile strains are compared directly to the FE model as experimental compressive strain measurements were affected by delamination within the carbon fibre layers. Single point/node comparison exhibited a good correlation with strain measures through increasing load application. The result is consistent throughout the increment in applied displacement. Strain measurements over a line along the metal thickness during the loading phase show that, as the applied displacement increases and reaches 20 mm the agreement between DIC and FE measurements improves as well. In addition, different areas were taken to average strain measurements and compare to FE. Results exhibit noticeable differences which are presumed to be due to the lack of a matrix failure mode within the FE model which would reduce the effective stiffness of the cylinder wall. However, despite these differences, results show good overall agreement.

The key overall conclusion of this work is that the use of embedded cohesive zone elements, together with appropriate constitutive laws for the materials, represents an effective approach for modelling the global and local structural response of metal–composite hybrid structures. This has particular significance for the prediction of damage tolerance and damage resistance of such structures. Furthermore, we believe that the detailed model-experiment comparison, include global and local measurements of deformation and damage is the key to ensuring effective model validation and calibration.

CRediT authorship contribution statement

Erick Montes de Oca Valle: Concept, Design, Analysis, Writing, Revision of the manuscript. **Mark Spearing:** Concept, Design, Analysis, Writing, Revision of the manuscript. **Ian Sinclair:** Concept, Design, Analysis, Writing, Revision of the manuscript. **Trevor Allen:** Concept, Design, Analysis, Writing, Revision of the manuscript. **Warren Hepples:** Concept, Design, Analysis, Writing, Revision of the manuscript.

Declaration of competing interest

The authors declare that they have no known competing financial interests or personal relationships that could have appeared to influence the work reported in this paper.

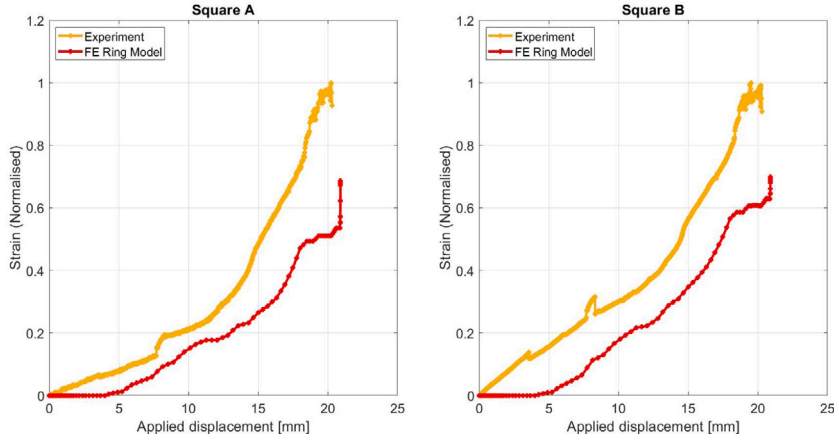

Fig. 16. Strain average measurement comparison: DIC vs FEA.

Data availability

The data that has been used is confidential.

Acknowledgements

We would like to thank Luxfer Gas Cylinders, UK for their financial support and constant help, which was key to success in the achievement of this publication. We also want to thank the National Council for Science and Technology (CONACYT) in Mexico, for the financial support provided, which made possible the development of this research.

References

[1] H. Barthelemy, M. Weber, F. Barbier, Hydrogen storage: Recent improvements and industrial perspectives, Int. J. Hydrogen Energy 42 (11) (2017) 7254–7262, http://dx.doi.org/10.1016/j.ijhydene.2016.03.178.

[2] A.E. Pavan, K.S. Ahmed, Effect of Constituent Shell, Int. J. Sci. Eng. Res. 9 (5) (2018) 112–118.

[3] S. Wakayama, S. Kobayashi, T. Imai, T. Matsumoto, Evaluation of burst strength of FW-FRP composite pipes after impact using pitch-based low-modulus carbon fiber, Composites A 37 (11) (2006) 2002–2010, http://dx.doi.org/10.1016/j.compositesa.2005.12.010.

[4] S. Kobayashi, M. Kawahara, Effects of stacking thickness on the damage behavior in CFRP composite cylinders subjected to out-of-plane loading, Composites A 43 (1) (2012) 231–237, http://dx.doi.org/10.1016/j.compositesa.2011.10.004.

[5] P. Blanc-Vannet, O. Bardoux, N. Alexandre, F. Nony, M. Barcikowski, R. Rybczyński, A. Maldachowska, P. Breuer, K. Lasn, A. Echtermeyer, F. Dahmene, S. Bittendiebel, Residual performance of composite pressure vessels submitted to mechanical impacts, in: Proceedings of 7th International Conference Hydrogen Safety (ICHS 2017), September, 2017, pp. 488–495.

[6] M. Weber, C. Devilliersa, N. Guillaud, F. Dau, B. Gentilleauc, F. Nony, S. Villalonga, D. Halm, Damage tolerance of compressed gaseous hydrogen composites vessels, in: 16th European Conference on Composite Materials, ECCM 2014, June, 2014, pp. 22–26.

[7] Y.-S. Kim, L.-H. Kim, J.-S. Park, The effect of composite damage on fatigue life of the high pressure vessel for natural gas vehicles, Compos. Struct. 93 (11) (2011) 2963–2968, http://dx.doi.org/10.1016/j.compstruct.2011.05.007.

[8] S.K. Ha, J.Y. Jeong, Effects of winding angles on through-thickness properties and residual strains of thick filament wound composite rings, Compos. Sci. Technol. 65 (1) (2005) 27–35, http://dx.doi.org/10.1016/j.compscitech.2004.05.019.

[9] F. Eggers, J.H.S. Almeida, C.B. Azevedo, S.C. Amico, Mechanical response of filament wound composite rings under tension and compression, Polym. Test. 78 (January) (2019) 105951, http://dx.doi.org/10.1016/j.polymertesting.2019.105951.

[10] R.A. Weerts, O. Cousigné, K. Kunze, M.G. Geers, J.J. Remmers, Assessment of contact-induced damage mechanisms in thick-walled composite cylinders, J. Reinf. Plast. Compos. 39 (17–18) (2020) 679–699, http://dx.doi.org/10.1177/0731684420923043.

[11] K.L. Alderson, K.E. Evans, Low velocity transverse impact of filament-wound pipes: Part 1. Damage due to static and impact loads, Compos. Struct. 20 (1) (1992) 37–45, http://dx.doi.org/10.1016/0263-8223(92)90010-A.

[12] J. Curtis, M.J. Hinton, S. Li, S.R. Reid, P.D. Soden, Damage, deformation and residual burst strength of filament-wound composite tubes subjected to impact or quasi-static indentation, Composites B 31 (5) (2000) 419–433, http://dx.doi.org/10.1016/S1359-8368(00)00014-7.

[13] T. Allen, S. Ahmed, W. Hepples, P.A. Reed, I. Sinclair, M. Spearing, A comparison of quasi-static indentation and low-velocity impact on composite overwrapped pressure vessels, J. Compos. Mater. 52 (29) (2018) 4051–4060, http://dx.doi.org/10.1177/0021998318774401.

[14] Z. Changliang, R. Mingfa, Z. Wei, C. Haoran, Delamination prediction of composite filament wound vessel with metal liner under low velocity impact, Compos. Struct. 75 (1–4) (2006) 387–392, http://dx.doi.org/10.1016/j.compstruct.2006.04.012.

[15] M.-G. Han, S.-H. Chang, Failure analysis of a Type III hydrogen pressure vessel under impact loading induced by free fall, Compos. Struct. 127 (2015) 288–297, http://dx.doi.org/10.1016/j.compstruct.2015.03.027, URL http://linkinghub.elsevier.com/retrieve/pii/S0263822315001993.

[16] M.G. Han, S.H. Chang, Evaluation of structural integrity of Type-III hydrogen pressure vessel under low-velocity car-to-car collision using finite element analysis, Compos. Struct. 148 (2016) 198–206, http://dx.doi.org/10.1016/j.compstruct.2016.03.060.

[17] S. Kobayashi, T. Imai, S. Wakayama, Burst strength evaluation of the FW-CFRP hybrid composite pipes considering plastic deformation of the liner, Composites A 38 (5) (2007) 1344–1353, http://dx.doi.org/10.1016/j.compositesa.2006.10.011.

[18] G. Perillo, F. Grytten, S. Sørbø, V. Delhaye, Numerical/experimental impact events on filament wound composite pressure vessel, Composites B 69 (2015) 406–417, http://dx.doi.org/10.1016/j.compositesb.2014.10.030.

[19] J. Zheng, Y. Hu, L. Ma, Y. Du, Delamination failure of composite containment vessels subjected to internal blast loading, Compos. Struct. 130 (2015) 29–36, http://dx.doi.org/10.1016/j.compstruct.2015.04.013.

[20] T.M. Allen, Damage Development and Post-Impact Performance of Composite Overwrapped Pressure Vessels Subjected to Low Velocity Impact (Ph.D. thesis), (March) University of Southampton, 2017.

[21] A. Turon, P.P. Camanho, J. Costa, C.G. Dávila, A damage model for the simulation of delamination in advanced composites under variable-mode loading, Mech. Mater. 38 (11) (2006) 1072–1089, http://dx.doi.org/10.1016/j.mechmat.2005.10.003.

[22] S.R. Hallett, P.W. Harper, Modelling delamination with cohesive interface elements, Numer. Model. Failure Adv. Composite Mater. (2015) 55–72, http://dx.doi.org/10.1016/B978-0-08-100332-9.00002-5.

[23] J.C. Ríos, E. Chomik, J.J. Balderrama, F. Cambiasso, E. Asta, Determination of Fracture Toughness J on Fiber-metal Laminate Type CARALL with Sheets of Aluminium 6061, Procedia Mater. Sci. 9 (2015) 530–537, http://dx.doi.org/10.1016/j.mspro.2015.05.026.

[24] E.V. González, P. Maimí, A. Turon, P.P. Camanho, J. Renart, Simulation of delamination by means of cohesive elements using an explicit finite element code, Comput. Mater. Contin. 9 (1) (2009) 51–92, http://dx.doi.org/10.3970/CMC.2009.009.051.

[25] A. Turon, C.G. Dávila, P.P. Camanho, J. Costa, An Engineering Solution for using Coarse Meshes in the Simulation of Delamination With Cohesive Zone Models, 2005, pp. 1–26, Nasa/Tm-2005-213547 March.

[26] R. Bigger, B. Blaysat, C. Boo, M. Grewer, J. Hu, A. Jones, M. Klein, K. Raghavan, P. Reu, T. Schmidt, T. Siebert, M. Simenson, D. Turner, A. Vieira, T. Weikert, A Good Practices Guide for Digital Image Correlation, Int. Digital Image Correlation Soc. (2018) 94, http://dx.doi.org/10.32720/idics/gpg.ed1, URL http://idics.org/guide/.